

Multi-Objective Evolutionary Design of Molecules with Enhanced Nonlinear Optical Properties

Dominic Mashak
 Southwestern University
 Georgetown, Texas, USA
 mashakd@southwestern.edu

Jacob Schrum
 Southwestern University
 Georgetown, Texas, USA
 schrum2@southwestern.edu

S.A. Alexander
 Southwestern University
 Georgetown, Texas, USA
 alexands@southwestern.edu

Abstract

Nonlinear optical (NLO) materials are essential for many photonic, telecommunication, and laser technologies, yet discovering better NLO molecules is computationally challenging due to the vast chemical space and competing objectives. We compare evolutionary algorithms for molecular design, targeting four objectives: maximizing the ratio of first-to-second hyperpolarizability (β/γ), optimizing HOMO-LUMO gap and linear polarizability to target ranges, and minimizing energy per atom. We encode molecules as SMILES strings and evaluate their properties using quantum-chemical calculations. We compare NSGA-II, MAP-Elites, MOME, a single-objective ($\mu + \lambda$) evolutionary algorithm, and simulated annealing. Quality diversity methods maintain archives across a measure space defined by atom and bond count, enabling the discovery of structurally diverse molecules. Our results demonstrate that NSGA-II consistently earns high scores in every objective, leading to high-quality molecules, but MOME does a better job exploring a wide range of possibilities, resulting in higher global hypervolume and MOQD scores. However, each method has strengths and weaknesses, and produced many promising molecules.

CCS Concepts

• Applied computing → Chemistry; • Computing methodologies → Molecular simulation.

Keywords

Multi-Objective optimization, Quality Diversity, Computational Chemistry

1 Introduction

Nonlinear optical (NLO) materials can modify the frequency, phase, and/or polarization of light [24, 26, 31]. Because these properties enable optical communication, optical computing, optical data storage, and optical switching devices, many research groups are actively seeking molecules with specific NLO properties [5, 6, 30]. Over the past few decades, the development of reliable black-box quantum-chemical programs has enabled theoretical chemists to evaluate the properties of NLO molecules solely from their structures.

Despite the commercial importance of NLO materials, the scientific literature contains only general guidelines as to which properties an ideal NLO material should have for a specific application. Most studies focus on a particular property, such as molecular first hyperpolarizability (β) [11, 12, 18, 32, 33]. In this paper, we consider an electro-optic modulator [24] as an example NLO device, and identify properties that a molecule must possess to function as an electro-optic modulator (Section 3). We seek molecules that optimize these properties using multiobjective optimization (MOO) [7],

quality diversity (QD) [25], multiobjective QD (MOQD) [27], single-objective evolution, and simulated annealing. Previous work [21] demonstrates that evolutionary algorithms can be used to search for molecules with large hyperpolarizabilities, but we apply a wider variety of approaches to a harder problem: finding molecules that simultaneously satisfy multiple, often conflicting, criteria.

Our results show that MOQD via the MOME algorithm [27] creates the best variety of molecules, covering many diverse niches while also maximizing hypervolume [41], but the multiobjective optimization algorithm NSGA-II [7] uncovers higher scores in each individual objective, providing a different set of trade-offs. Single-objective methods optimize our main objective of first-to-second hyperpolarizability ratio at the expense of other objectives, but the diversity that is fostered by the QD method MAP-Elites [25] allows it to perform better on a wider range of objectives, even though it is not aware of them. All of these approaches provide an interesting variety of potential NLO materials for further study.

2 Related Work

Various search methods have been applied to molecular design. Simulated annealing and evolutionary algorithms have been used to optimize molecular hyperpolarizabilities with semi-empirical quantum chemistry [20, 21], representing molecules with SMILES strings [39], which we also use in our experiments (Section 4.1).

Though effective, such optimization techniques generally ignore other aspects of design that impact solution usefulness. In contrast, quality diversity (QD) approaches [4, 25] seek diverse collections of artifacts while also maximizing fitness. Graph-based elite patch illumination (GB-EPI [38]) is a QD approach that was applied to small-molecule drug rediscovery benchmarks. GB-EPI evolves graph-based representations instead of SMILES strings, while our experiments combine SMILES with QD.

A separate limitation of standard optimization is its focus on a single objective. Multiobjective Pareto-based optimization addresses this by exploring trade-offs between competing objectives rather than seek diversity in design space, and has also been applied to evolving molecules for small-molecule drug design [10, 37].

We apply QD and multiobjective (MO) techniques, along with others, to the problem of discovering molecules for the design of an effective electro-optic modulator.

3 Defining an Effective Electro-Optic Modulator

When intense laser light strikes an electro-optic (EO) modulator, the molecular response to the electric field [26] determines output properties via polarizability tensors α , β , and γ . An effective EO modulator requires balancing four properties. First, EO modulators exploit the Pockels effect [31], a second-order NLO process

proportional to hyperpolarizability (β); high β enables stronger modulation and smaller devices, while γ should be small enough to avoid self-phase modulation and optical Kerr effects [31] yet sufficient for intense-field performance [31]. Second, linear polarizability (α) must be balanced: high values provide strong charge transfer (beneficial for β and γ), but excessive α causes absorption, dispersion, or aggregation. Third, the HOMO-LUMO gap (ΔE) controls electron mobility and optical transparency; small gaps risk visible-light absorption and thermal damage, while large gaps ensure transparency but weaken NLO activity. Fourth, molecules must be thermodynamically stable. These properties are calculable via quantum-chemical programs, which we combine with evolutionary algorithms to search for optimal EO modulators.

4 Methods

SMILES strings representing molecules are evolved using MOO, QD, MOQD, and single-objective evolution, and compared with simulated annealing. The properties of candidate molecules are calculated using the PySCF library [34].

4.1 SMILES String Encoding

SMILES (Simplified Molecular Input Line Entry System [39]) encodes molecular structures as ASCII strings. We restrict molecules to C, N, O, and H atoms, focusing on organic NLO candidates, following prior work [21]. Atoms are represented by atomic symbols; organic atoms (C, O) omit brackets and use implicit hydrogens based on valence. Bonds are limited to single (implicit $-$) and double ($=$) bonds. Branches are represented by parentheses at the attachment point (e.g., C-C(-O)-O), and rings by matching digit labels (e.g., C1-C-C-C-C1). Canonical SMILES from RDKit [17] ensure unique representations for comparison and deduplication.

This encoding enables our integration with quantum chemistry packages for evaluation, as SMILES strings can be directly converted to molecular geometries for calculations of hyperpolarizabilities and other properties.

4.2 Calculating Chemical Properties

Candidate molecules are evaluated by converting canonical SMILES to molecular geometries using RDKit [17], then computing quantum-chemical properties with PySCF [34], a Python library for *ab initio* electronic structure calculations via Hartree-Fock (HF).

We use HF/3-21G based on systematic benchmarking [22] showing perfect pairwise ranking agreement (100% consistency ordering molecules by β) against experimental hyperpolarizabilities [12]. While absolute errors exist, preserving relative ordering is critical for elitist/tournament selection in evolutionary algorithms.

Computed values yield the four objectives in Section 5.2. Molecules with invalid geometries or SCF failures receive the worst fitness values and are excluded per bounds in Section 7.2.

4.3 Multiobjective Optimization

Molecular design inherently involves competing objectives. Rather than optimize objectives independently or combine them, multiobjective optimization [40] simultaneously optimizes multiple objectives to produce a set of trade-off solutions.

A solution \vec{x}_1 Pareto dominates \vec{x}_2 ($\vec{x}_1 \prec \vec{x}_2$) if \vec{x}_1 is no worse than \vec{x}_2 in every objective and strictly better in at least one.

$$\vec{x}_1 \prec \vec{x}_2 \Leftrightarrow \forall i : f_i(\vec{x}_1) \leq f_i(\vec{x}_2) \wedge \exists j : f_j(\vec{x}_1) < f_j(\vec{x}_2) \quad (1)$$

This definition assumes minimization, but maximization is achieved by flipping inequalities. The Pareto front is the set of all non-dominated solutions, representing the optimal trade-off surface between objectives.

4.4 Quality Diversity

Quality diversity (QD) algorithms seek not just high-performing solutions, but a diverse collection of high-performing solutions exhibiting different properties [25]. Rather than converge to a single optimum or Pareto front, QD methods generally maintain an archive of solutions that excel across various niches of design space.

Formally [9], QD methods depend on a fitness function and k measure functions $m_i : \mathcal{S} \rightarrow \mathbb{R}$. \mathcal{S} is the space of candidate solutions (SMILES strings). Each measure function calculates a solution property relevant to its design, but distinct from fitness. A k -dimensional archive is discretized into bins with a chosen level of granularity, determining how novel a solution has to be in order to compete within a different evolutionary niche.

The measure functions determine where a solution fits in the archive. Each bin holds one solution; higher fitness solutions replace worse ones, but solutions that discover empty bins are accepted regardless of fitness. QD algorithms maximize both coverage of the archive and overall quality of solutions. However, standard QD assumes only one fitness function determines solution quality.

4.5 Multiobjective Quality Diversity

MOQD algorithms [27] combine the complementary strengths of MOO and QD. While MOO methods optimize toward a Pareto front without regard to diversity in measure space, and QD algorithms maintain diversity but optimize only a single objective, MOQD pursues both goals: discovering diverse solutions that represent optimal objective trade-offs within each niche.

MOQD maintains an archive across the measure space while preserving multiple Pareto-optimal solutions in each niche. The main modification to standard QD is allowing each archive bin to store a Pareto front [27] consisting of mutually non-dominated solutions that share measure characteristics, but represent different objective trade-offs.

5 Experiment

Our code is available on GitHub at (will be public at a future date). These experiments focus on comparing different approaches to evolving molecules for their NLO properties.

5.1 Algorithms

We compare five algorithms encompassing single-objective, MO, QD, and MOQD approaches.

Non-dominated Sorting Genetic Algorithm II (NSGA-II) [7] uses Pareto dominance ranking and crowding distance for selection. Solutions are sorted into non-dominated fronts, with binary tournament selection favoring better fronts. Crowding distance promotes

spread along the Pareto front by preferring solutions in less populated objective space regions.

Multi-dimensional Archive of Phenotypic Elites (MAP-Elites) [25] maintains an archive of elite solutions across a discretized measure space. Each bin stores the fittest solution for its niche, maintaining diversity via spatial partitioning. During evolution, candidates are generated via mutation of randomly selected archive members, and assigned to bins based on their measures. If a bin is empty, the candidate fills it. If occupied, the candidate replaces the current occupant only if it has superior fitness. This process continues and fills the archive with diverse, high-quality solutions.

Multiobjective MAP-Elites (MOME) [27] extends MAP-Elites by storing local Pareto fronts within each archive bin rather than single elites. Each bin maintains a mutually non-dominated Pareto front of objective trade-offs. Solutions are generated as with MAP-Elites, and assigned to bins based on their measures. They remain in their assigned bin if it is empty, or if they are non-dominated with respect to the previous occupants. Old occupants are only discarded if they are dominated by new occupants.

Simple $(\mu + \lambda)$ elitist selection [1] is a single-objective method where μ parents generate λ offspring per generation, and the best μ individuals from the combined parent-offspring pool are retained for the next generation. This elitist strategy is a simple baseline.

Simulated Annealing (SA) [8, 36] is a non-evolutionary method that maintains a single solution, accepting improvements unconditionally and worse solutions with probability $\exp(\Delta E/T)$ via the Metropolis criterion [23], where ΔE is the fitness difference and T is the *temperature*. Large T values promote exploration while small values favor exploitation.

5.2 Objectives

MO approaches target four objectives:

- First-to-Second Hyperpolarizability Ratio (β/γ): We maximize this ratio to favor strong second-order responses relative to third-order effects, promoting efficient frequency conversion without competing third-order processes. β is computed via second-order finite differences on dipole moments at 27 field configurations ($\pm h = 0.001$ a.u.), yielding all 27 β_{ijk} tensor components [2, 13, 22]. Similarly, γ uses fourth-order finite differences on total energy at field strengths $0, \pm h, \pm 2h$ along each axis; mean γ averages the three diagonal components γ_{iiii} .
- Linear Polarizability Range Deviation (f_α): Large α indicates high electronic mobility, but excessive values cause optical losses and reduced photostability [26]. We compute α via central finite differences on dipole moments with fields $\pm h$ along each axis: $\alpha_{ii} \approx [\mu_i(+h) - \mu_i(-h)]/(2h)$, then average tensor components. Targeting 100–500 a.u. (common in NLO materials with strong β), we minimize:

$$f_\alpha = \max(0, 100 - \alpha) + \max(0, \alpha - 500) \quad (2)$$

- HOMO-LUMO Gap Range Deviation ($f_{\Delta E}$): Gaps near 2 eV provide strong charge-transfer and high β but risk red/near-IR absorption; gaps above 4 eV ensure visible transparency

but reduce β . Targeting 2–4 eV for visible/near-IR applications, we minimize:

$$f_{\Delta E} = \max(0, 2 - \Delta E) + \max(0, \Delta E - 4) \quad (3)$$

- Energy per Atom (E_{total}/N_{atoms}): Total energy from PySCF’s geometry-optimized HF calculation, divided by atom count, proxies thermodynamic stability. Minimizing this encourages compact, low-strain geometries resisting decomposition, practical for synthesizable NLO materials. Positive values indicate SCF failures or strained geometries, so we reject those molecules (see Section 7.2 and 8).

NSGA-II and MOME optimize all objectives; $(\mu + \lambda)$, MAP-Elites, and simulated annealing optimize only β/γ . This isolates the primary NLO metric to test whether high second-order responses correlate with desirable secondary objectives or require MOO. We avoid weighted sums due to scaling and hyperparameter sensitivity.

5.3 Diversity Measures and Archives

The archives used by MAP-Elites and MOME to characterize molecular diversity are based on two measures:

- m_1 : Number of Atoms: The count of heavy (non-hydrogen) atoms in the molecule, discretized into bins. Hydrogens are typically implicit in SMILES notation and are not counted. Range $(\min_1, \max_1) = (5, 30)$.
- m_2 : Number of Bonds: The count of covalent bonds in the molecular graph between heavy atoms, similarly discretized into bins. Bonds to implicit hydrogen atoms are not counted. Each bond is counted once, regardless of type (single and double bonds both count as 1). Range $(\min_2, \max_2) = (4, 32)$.

We utilize square $M \times M$ grid-shaped archives, where the index b_i along dimension i is:

$$b_i = \left\lfloor \frac{m_i - \min_i}{\max_i - \min_i} \times M \right\rfloor \quad (4)$$

The value of M depends on the binning scheme. There are two:

- Coarse: $M = 10$: A 10×10 grid (100 bins).
- Fine: $M = 20$: A 20×20 grid (400 bins).

This approach does not provide a one-to-one mapping between measure values and bins. Some adjacent measure values map to the same bin, even in the fine scheme. Molecules with measure values beyond the boundaries are assigned to the nearest bin.

The coarse archive has fewer bins, storing fewer molecules and increasing competition within each niche. The possible benefit of fewer bins is that low fitness individuals are less likely to persist and be selected for mutation. The impact of archive granularity depends on how evolutionary stepping stones are distributed in measure space. A fine-grained archive might be better if important stepping stones lie across boundaries that are merged into a single bin in a coarse archive. This is one of several empirical questions we explore with our experiments. Also, note that with MOME, the Pareto fronts in each bin can have multiple molecules, so different molecules on the same front in a coarse archive may have measures that would result in separate placement in a fine-grained archive.

Regardless of the granularity, many bins in both archive types represent properties that are chemically impossible to fulfill, such as having more bonds than atoms.

5.4 SMILES String Mutations

We employ seven mutation operators [20, 21] that stochastically modify canonical SMILES strings using RDKit [17], restricting mutations to {C, N, O} atoms with { -- , = } bonds. Each mutation converts the parent SMILES to an editable molecular graph, applies the modification, and regenerates a canonical SMILES. Invalid results are discarded and retried up to 20 times before attempting a different mutation. The seven operators are:

- Change Bond Type: Toggles single/double bonds respecting valence (e.g., $\text{C=C--N--O} \rightarrow \text{C=C--N=O}$)
- Insert Atom: Breaks a bond and inserts C, N, or O (e.g., $\text{C=C--N--O} \rightarrow \text{C=C--O--N--O}$)
- Add Branch: Attaches a new atom to an existing one (e.g., $\text{C=C--N--O} \rightarrow \text{C=C}(\text{--O})\text{--N--O}$)
- Delete Atom: Removes an atom and reconnects the graph (e.g., $\text{C=C--N--O} \rightarrow \text{C=C--O}$)
- Change Atom Type: Substitutes atom element (e.g., $\text{C=C--N--O} \rightarrow \text{C=C--N--C}$)
- Add Ring: Connects non-adjacent atoms to form a cycle (e.g., $\text{C=C--N--O} \rightarrow \text{C1=C--N--O1}$)
- Delete Ring Bond: Opens a ring by removing one bond (e.g., $\text{C1=C--N--O1} \rightarrow \text{C=C--N--O}$)

Each child (except in simulated annealing) receives one to three randomly selected mutations. Simulated annealing generates one child per mutation type.

6 Algorithmic Settings

Each algorithm evaluates approximately 2,000 molecules. Simulated annealing starts from one molecule, applies all seven mutations per iteration for 285 iterations (1,996 evaluations), with exponential cooling from $T_{\text{initial}} = 100$ to $T_{\text{min}} = 0.01$ at rate $\alpha = 0.95$.

NSGA-II and $(\mu + \lambda)$ use $\mu = \lambda = 20$ over 100 generations (2,020 evaluations) with tournament selection ($k = 3$).

MAP-Elites and MOME seed archives with 50 random molecules, then mutate randomly selected archive members for 100 generations of 20 evaluations each (2,050 total).

All experiments use 20 random seeds. Initial populations are generated from common scaffolds (e.g., C, C=C, C-C-N) with multiple random mutations applied to create valid, unique molecules. Only C, N, O, and H atoms are permitted. Single and double bonds are allowed; triple bonds are forbidden. Molecules must contain 5–30 heavy atoms (non-hydrogen) and must form a single connected component (no disconnected fragments).

7 Results

Algorithms are compared in terms of the following results produced by each of their 20 distinct runs using different random seeds. In general, results across runs do not follow a normal distribution and have very high performing outliers, so we favor the use of median scores to compare typical algorithm performance.

7.1 Median Best Objective Scores

Across all seeds of each algorithm, the median of the *best* objective scores ever encountered in each objective are in Figure 1. The best objective score after a certain number of evaluations in a given run

is either the highest or lowest score, depending on the objective, across all molecules produced up to that point.

The incredibly high β/γ scores of plain $(\mu + \lambda)$ selection stand out, but when combined with poorer scores in other objectives, these molecules actually prove to be so unstable as to be practically worthless. The unfortunate conclusion is that optimizing exclusively based on hyperpolarizability scores allows evolution to cheat in a way that bypasses the intended application of these molecules. The push for diversity in MAP-Elites is likely what helps it avoid this trap, despite also being a single-objective method. Simulated annealing does surprisingly well in $f_{\Delta E}$ score, despite this not being the objective it was explicitly optimizing, but at the cost of f_α and $E_{\text{total}}/N_{\text{atoms}}$. The high $E_{\text{total}}/N_{\text{atoms}}$ indicates severe instability.

The next highest β/γ scores come from NSGA-II, which also achieves top performance in the other three objectives, tying for best in f_α , being the only evolutionary method with an optimal median for $f_{\Delta E}$, and being the clear best in $E_{\text{total}}/N_{\text{atoms}}$. These results make sense given the MO nature of NSGA-II.

7.2 Median Global Hypervolume

Regardless of whether evolution is single- or multi-objective, a Pareto front can be computed over all molecules with our four objectives. Therefore, we calculate a Pareto front across all molecules generated so far in each run, and use it to calculate the hypervolume using pymoo [3]. Hypervolume (HV) measures the region (Lebesgue measure) dominated by the Pareto front with respect to a reference point dominated by all points [41]. HV is a single metric measuring the quality of trade-offs in the front.

However, hypervolume is sensitive to differences in objective scale and to extreme outliers [41], making normalization of objective scores necessary. Our quantum chemistry calculations sometimes produced extremes that were impossible, which needed to be discarded (see Section 8). Based on analysis of what evolution discovered, and informed by knowledge of what is reasonable both chemically and physically, we normalized each objective score based on the following ranges:

- β/γ : [0, 9419] (unitless)
- f_α : [0, 440] (a.u.)
- $f_{\Delta E}$: [0, 16] (eV)
- $E_{\text{total}}/N_{\text{atoms}}$: [−75, 0] (Hartree)

These values scaled scores to the range [0, 1] before performing the HV calculation with a reference point of $\vec{0}$.

Figure 2a shows median hypervolume scores across evaluations. We call these *global* hypervolumes to distinguish them from scores associated with MOQD (Section 7.5). MOME_F performs best by this metric, which makes sense given that it is explicitly multiobjective and maintains diverse niches, which helps with coverage of objective space. In contrast, the relatively poor performance of MOME_C is surprising. The MOME_C results suggest an overall quality penalty from having fewer bins to support more fine-grained niches.

Below MOME_F are methods roughly tied for second place in terms of median HV: $(\mu + \lambda)$, NSGA-II, and MAP-Elites_C. NSGA-II’s performance makes sense given that MO algorithms are meant to increase HV. The $(\mu + \lambda)$ result hides the fact that this HV score is primarily due to high β/γ , and not balanced across objectives.

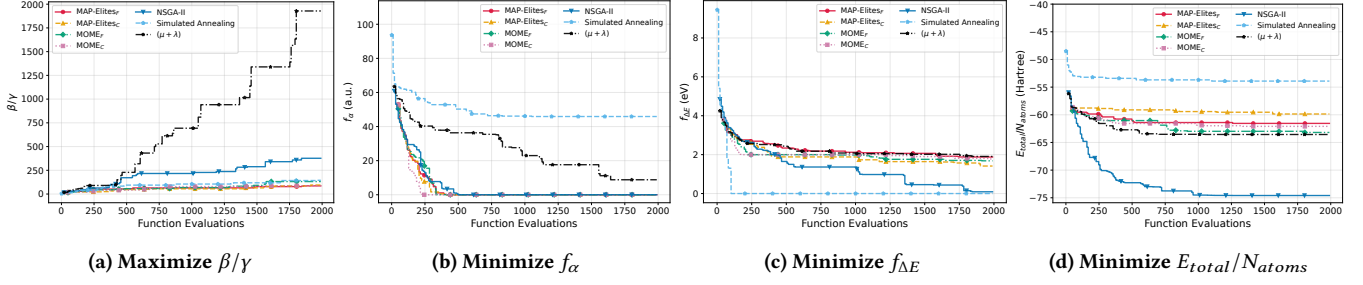


Figure 1: Median Best Objective Scores Across 20 Runs of Each Algorithm: (a) Median first-to-second hyperpolarizability ratio. High values are better, so $(\mu + \lambda)$ outperforms all others by a large margin, including other single-objective methods, though NSGA-II is clearly second-best. (b) Median linear polarizability range deviation. All but simulated annealing and $(\mu + \lambda)$ quickly reach a perfect minimal score of 0, though $(\mu + \lambda)$ at least gets close. (c) Median $f_{\Delta E}$ range deviation. NSGA-II and simulated annealing tie for best with perfect minimal scores of 0, which the other algorithms do not reach. The single-objective methods were not aware of this objective, so their poorer performance is not surprising, but MOME's performance is slightly disappointing. However, these are only median scores; some MOME runs reach the perfect score, but less than half. (d) Median energy per atom. NSGA-II is clearly the best at minimizing this objective, with most other methods clustering closer together, including the single-objective methods that were unaware of this objective. Only simulated annealing is exceptionally poor.

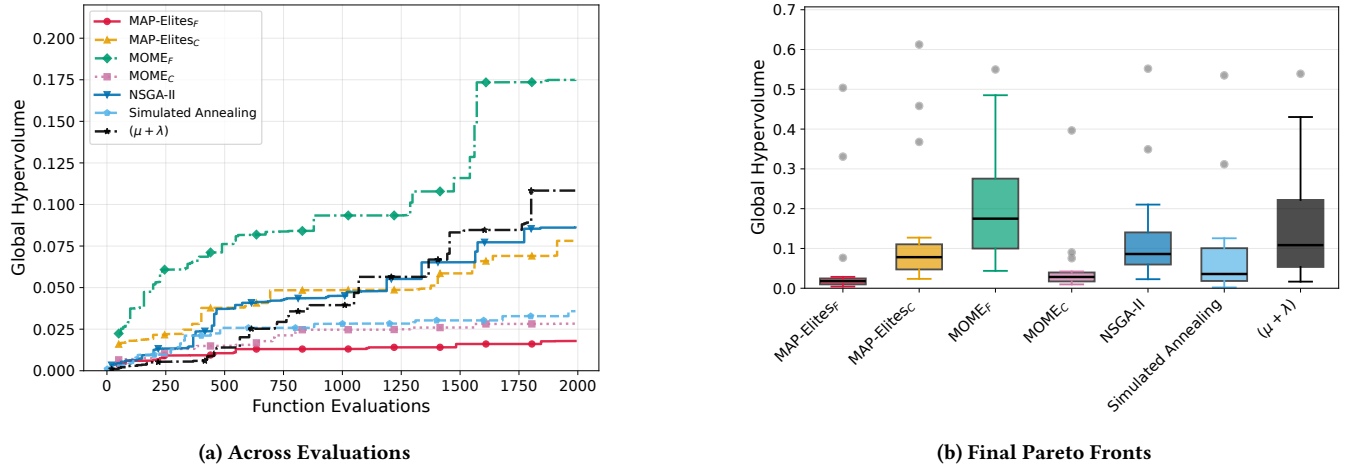


Figure 2: Global Hypervolume Scores Across 20 Runs of Each Algorithm: (a) Median hypervolume scores for each algorithm across function evaluations. MOME_F is the best, followed by a cluster of $(\mu + \lambda)$, NSGA-II, and MAP-Elites_C, before algorithms start to bunch together near the bottom. (b) Box-and-whisker plots of hypervolume scores for final Pareto fronts. The lower quartile, median, and upper quartile are the lower boundary, center line, and upper boundary of each box respectively, and the whiskers denote the furthest points within $1.5IQR$ of the nearest quartile, where IQR is the interquartile range. Points outside of the whiskers are outliers, of which there are many. However, MOME_F and $(\mu + \lambda)$ both have high upper quartiles, and spread more across the range of higher scores.

The high performance of MAP-Elites_C contrasts with MOME: MAP-Elites_C is far superior to MAP-Elites_F (worst global HV), but the coarse vs. fine relationship is opposite with MOME. A fine-grained archive is beneficial to MOME, but a detriment to MAP-Elites, likely due to the specific objectives and measures used. Changes in atom or bond count are more likely to have a direct impact on HOMO-LUMO gap, energy per atom, and linear polarizability, which are tied to the objectives that MAP-Elites does not directly optimize. Therefore, each MAP-Elites_C bin forces molecules with differing atom and bond counts to compete on β/γ , while allowing variation in unoptimized objectives to persist among high-performing solutions. This can increase global hypervolume by retaining non-dominated trade-offs that are a byproduct of optimizing β/γ . In contrast, coarse MOME archives increase domination

pressure in each bin, causing trade-offs between structurally dissimilar molecules to cut off possible stepping stones, reducing the diversity of molecules for further exploration.

Figure 2b focuses only on results at the end of evolution, but shows spread across all 20 runs of each algorithm with box-and-whisker plots. There are many high outliers. The only algorithms whose scores are consistently in a higher range are MOME_F and $(\mu + \lambda)$. The high performance of MOME_F makes sense for the reasons described above, whereas the high HV scores for $(\mu + \lambda)$ depend primarily on the contribution of its high β/γ scores, as shown previously. Even though hypervolume is a measure of space dominated by *all* objectives, the β/γ scores for $(\mu + \lambda)$ are so high that they compensate for poor scores in the other objectives.

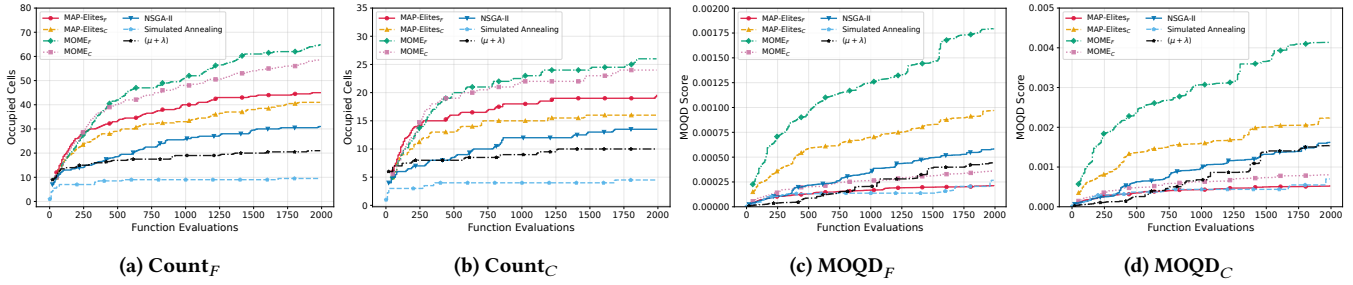


Figure 3: Fine-grained and Coarse Archive Median Scores Across 20 Runs of Each Algorithm: (a) Median bin count with fine-grained binning. Unsurprisingly, QD methods fill more bins than non-QD approaches, and simulated annealing performs the worst. Fine-grained QD methods occupy slightly more bins than their coarse counterparts. (b) Median bin count with coarse binning. The scale is different with a coarse archive, but results are qualitatively identical to the fine-grained archive results. Interestingly, fine-grained QD methods still occupy more bins than their coarse counterparts. (c) Median MOQD with fine-grained binning. MOME_F is clearly superior, followed distantly by MAP-Elites_C, then NSGA-II, before the rest cluster more tightly together. (d) Median MOQD with coarse binning. Qualitatively similar to the fine-grained MOQD results, except that $(\mu + \lambda)$ demonstrates a significant jump in MOQD score near the end of evolution that ties it with NSGA-II.

7.3 Fine and Coarse Median Archive Bin Count

With QD methods, it is desirable to know how much of the measure space is covered by solutions. For algorithms with archives, we simply count the number of occupied bins, but the comparison is more complicated when different methods use different binning schemes, or do not use an archive at all.

For the sake of fair comparison, we present both the number of bins that would be occupied in a fine-grained binning scheme Count_F (Figure 3a), and the number of bins that would be occupied in a coarse binning scheme Count_C (Figure 3b). Note that Count_F can be calculated for QD methods that evolve with a coarse archive and vice-versa. These quantities are also calculated for algorithms that do not use an archive, using the stream of generated molecules to create the archive after the algorithm is finished. Each Count metric is the number of occupied bins in an archive of the appropriate type after a given number of molecule evaluations.

Fine and coarse archive counts exhibit differences in scale but are not qualitatively distinct. Each exhibits the same ordering of algorithms and similar spacing between each. QD/MOQD methods explicitly support diversity, and thus occupy more bins than non-QD algorithms. Simulated annealing is especially poor in this metric, since it does not even use a population, hindering diversity.

Interestingly, fine-grained versions of MOME and MAP-Elites fill more bins in the coarse archive than the coarse versions, but the margins are small. Similarly, MOME with a given binning scheme occupies slightly more bins than MAP-Elites with that same binning scheme in both the coarse and fine cases.

7.4 Fine and Coarse Median QD Score

Single-objective QD algorithms use QD score [28] to measure success. QD score is the sum of scores in the one objective across occupied bins in an archive, meaning that QD score increases when more bins are occupied and when objective scores in occupied bins improve. Generating more and better solutions increases QD score.

Fine and coarse archives are used to calculate QD score according to each objective. We add the stream of generated molecules to an archive, and only allow a molecule in an occupied bin to be replaced if the new molecule has a better score in the objective of interest.

Figure 4 shows QD scores associated with each objective for fine-grained archives. Results for coarse archives are qualitatively identical, so are excluded. QD scores for β/γ (Figure 4a) are qualitatively similar to the raw β/γ scores (Figure 1a). QD scores based on the remaining objectives demonstrate the strengths of MOME: fine-grained and coarse versions excel in these objectives.

Though worse than MOME for $(f_\alpha)_F$ and $(f_{AE})_F$, MAP-Elites earns surprisingly high QD scores in these objectives, which it was not aware of, and MAP-Elites_F achieves the best scores in $(E_{total}/N_{atoms})_F$. Even though NSGA-II explicitly optimizes all objectives, MAP-Elites does better in these objectives by encouraging diversity with β/γ as the only objective. In contrast, $(\mu + \lambda)$ and simulated annealing perform poorly in objectives they were unaware of, due to lack of awareness and lack of pressure to diversify.

7.5 Median Multiobjective QD Score

The paper introducing MOME also introduced the MOQD score, or multiobjective QD score [27]. Recall that MOME bins can contain multiple solutions representing a Pareto front across objectives. Because HV represents the quality of a Pareto front, the quality of a MOME bin is the hypervolume of that bin, and MOQD score is the sum of all hypervolumes across all occupied bins in the archive.

Although this metric was developed for MOME, it can be applied to any algorithm given a stream of molecules. Now molecules are only added to occupied bins if they are non-dominated. Thus, even for single-objective QD algorithms and archive-free methods, MOQD_F (Figure 3c) and MOQD_C (Figure 3d) can be calculated.

MOME_F is vastly superior in both fine-grained and coarse archives, which is consistent with global HV results. MAP-Elites_C is second best, being far below MOME_F. Next comes NSGA-II followed by the rest, though in the coarse case $(\mu + \lambda)$ actually catches up to NSGA-II before the end of evolution. Still, the MOQD scores of $(\mu + \lambda)$ are much lower than its global hypervolume scores, indicating that its high HV depends on a cluster of structurally similar molecules that do not occupy much of measure space (Section 7.6).

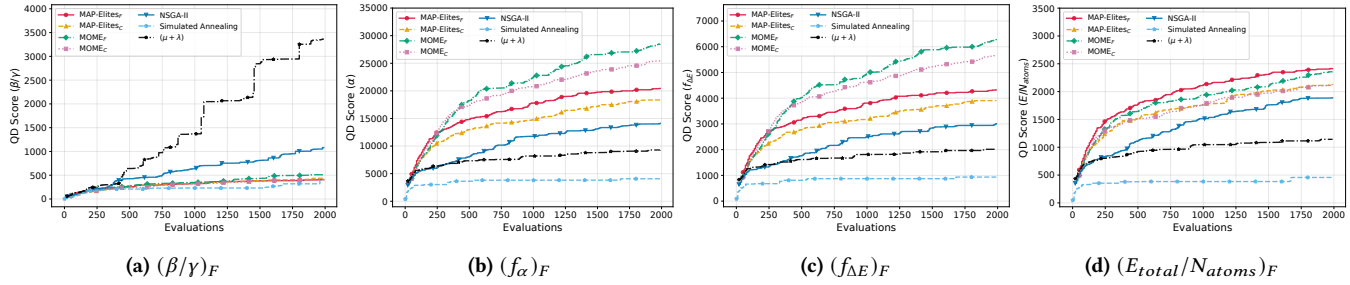


Figure 4: Fine-grained Archive Median QD Scores by Objective Across 20 Runs of Each Algorithm: (a) Median QD for first-to-second hyperpolarizability ratio using fine-grained binning. Qualitatively similar to raw objective scores for β/γ (Figure 4a), with strong performance by $(\mu + \lambda)$ and NSGA-II in second place. (b) Median QD for linear polarizability range deviation using fine-grained binning. Both MOME approaches perform the best, with MAP-Elites approaches beneath them, and NSGA-II trailing close behind, beating $(\mu + \lambda)$ and simulated annealing. (c) Median QD for HOMO-LUMO gap range deviation using fine-grained binning. Qualitatively similar to the $(f_\alpha)_F$ results. (d) Median QD for energy per atom using fine-grained binning. The MOQD and QD methods are more tightly clustered with NSGA-II near the top, but $(\mu + \lambda)$ is still far behind and simulated annealing is far below that.

7.6 Mega Archive Hypervolume Heatmaps

To capture overall performance, we create MOME-style archives that combine results across all 20 runs of each algorithm. Specifically, all of the molecules generated from all runs of a given algorithm are added to both a fine (Figure 5) and coarse (Figure 6) archive, and the typical MOME rules of placement according to measure values and non-dominance apply. We then show the hypervolumes of individual bins in heatmaps.

All heatmaps portray a diagonal slash through the archive, because bond count and atom count are strongly correlated, but the length and width of this slash varies. HV scores are generally low across most bins in each archive, with some rare bright spots.

The $(\mu + \lambda)$ archives show much less coverage, but more bright spots: these all correspond to unusually high β/γ scores. Simulated annealing has a fairly thick streak across the archive, despite low scores in many metrics above. However, the metrics above were median scores, indicating that the coverage seen in Figures 5a and 6a are the combination mostly disjoint archives from the separate runs.

MAP-Elites_C has high MOQD and global HV scores, but the archives indicate that a large portion of this may be attributable to one very bright bin. MAP-Elites_F has slightly less coverage, but much worse quality across most bins, explaining its lower scores.

MOME_F has board coverage, and many bins with moderate to high HV scores, which is consistent with its high MOQD and global HV scores. It is interesting that MOME_F has the highest coverage, global HV, and MOQD scores, even though these archives show that its coverage does not extend to the top-right of the archive as other methods do. MOME_C extends to the top right, but performed worse in all earlier metrics. It is once again important to point out that the earlier metrics were median scores, and that the archives here combine results across all runs, thus indicating that other methods do not span the whole archive from corner to corner consistently, whereas MOME_F does consistently cover the region shown in Figures 5e and 6e

NSGA-II archives (Figures 5g and 6g) extend to the top right, but are very thin and lacking in bright spots. The lack of bright spots explains NSGA-II’s low MOQD scores, and indicates that its moderately high global HV scores must depend on Pareto fronts

composed of molecules from different archive bins as opposed to molecules clustered in any one bin.

8 Discussion and Future Work

This work examines the efficacy of using single-objective, multiobjective, quality diversity, and MOQD algorithms to generate electro-optic modulators with an ideal set of properties. Our calculations show that several of these algorithms produce a diverse collection of molecules that satisfy the multiple criteria we set. In future research we plan to explore other variants of our more effective algorithms to determine how to improve the generation of molecules with specific properties.

Sometimes the quantum chemistry calculations described in Section 4.2 fail, producing physically impossible results. Some of these extreme outlier results were not caught until after our experiments were completed, but we removed these extreme cases from the results analysis. For example, the total energy per atom E_{total}/N_{atoms} should not be positive, but positive values were calculated for some molecules (+668,405 Hartree in one case). There was even one molecule with an excessively high β/γ ratio over 70,000, which is impossible because it violates quantum sum rules via the Kuzyk limit [14–16, 29]. These anomalies come from SCF convergence failures in the HF/3-21G calculations when applied to highly strained molecular geometries. Such molecules can exhibit a multi-reference character that the single-determinant Hartree-Fock theory cannot adequately describe [35]. Rather than representing exceptional molecular properties, these values indicate limitations of the computational method, and their inclusion would artificially inflate apparent algorithm performance.

Despite achieving the highest β/γ ratios among all algorithms and more consistently high global HV scores, $(\mu + \lambda)$ selection had poor overall performance due to its mediocre scores in other objectives, and low performance on Count and MOQD metrics. Even the β/γ ratios are somewhat questionable, as they reach values in the thousands which are theoretically possible but implausible. Although we retained these results in our analysis, they are another reason why $(\mu + \lambda)$ may not be as successful as it seems. The algorithm converges to a narrow region of chemical space with only smaller molecules that maximize the primary objective while

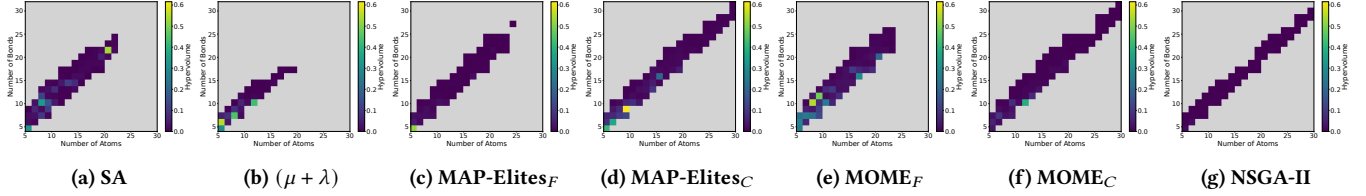


Figure 5: Fine-grained Mega Archive Hypervolume Heatmaps: Fine-grained archives that combine solutions from each algorithm across all 20 seeds, with heat scale showing each bin’s HV score. The x-axis is the atom count and the y-axis is the bond count.

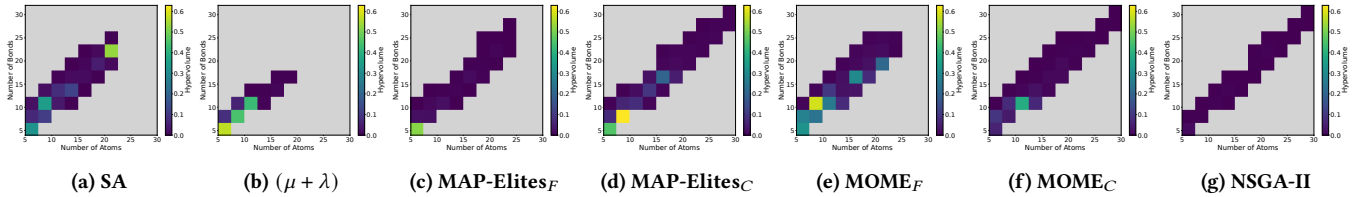


Figure 6: Coarse Mega Archive Hypervolume Heatmaps: Coarse archives that combine solutions from each algorithm across all 20 seeds, with heat scale showing each bin’s HV score. The x-axis is the atom count and the y-axis is the bond count.

neglecting secondary objectives. Notably, $(\mu + \lambda)$ solutions showed awful f_α compared to others that achieved perfect targeting of 0 a.u. The large f_α values indicate molecules that possibly exhibit increased optical absorption or dispersion, rendering them unsuitable as practical EO modulators despite strong nonlinear responses. This demonstrates that high performance on a single metric can be misleading when the application requires molecules satisfying multiple property constraints simultaneously.

NSGA-II performed well on all objectives in isolation, and was second only to $(\mu + \lambda)$ in terms of β/γ ratios. It also performed moderately well in terms of global HV, Count metrics, and MOQD scores. As a multiobjective algorithm, it produced more promising molecules exhibiting useful tradeoffs. One example is the molecule [O-][N+](O)OOONOCCOO[N+], which exhibits a linear topology dominated by oxygen-nitrogen linkages, including peroxide bridges (O-O-O) and nitro oxide functional groups. The structure achieves perfect targeting of the f_α constraint (0 a.u.), near-zero f_{AE} (0.80 eV), low E_{total}/N_{atoms} of -65.67 Hartree, and a β/γ ratio of 129.15, suggesting favorable NLO response characteristics [12].

MOME’s isolated median objective scores are middling, but MOME_F has the best median global HV, Count metrics, and MOQD scores. MOME also performs well on individual QD scores for all objectives except β/γ ratio, but this is an important objective. It is therefore hard to claim unequivocal success. It produces a broader range of molecules to investigate than any other method, and those molecules provide good coverage across the range of objectives. The molecule [C-][N+](N)=C(C)C(NN=C=N)C(=N)N=C=CON=CCC=C is a promising example, exhibiting: $\beta/\gamma = 134.20$, $f_\alpha = 14.27$ a.u., $f_{AE} = 3.87$ eV, and $E_{total}/N_{atoms} = -46.10$ Hartree. This molecule features an extended π -conjugated backbone incorporating multiple nitrogen heterocycles, carbodiimide groups (N=C=N), and a terminal vinyl ether moiety (ON=CCC=C). The ylide-type charge separation ([C-][N+]) at the molecular terminus, combined with the cumulated double bond systems, creates a push-pull electronic architecture characteristic of high-performance NLO chromophores [19]. Because of the numerous trade-offs and the differing compositions of molecules, many could be useful despite not having the highest

scores among all possibilities. In general, this is the promise of QD methods in general, and of MOQD methods in particular. They provide useful options for scientists to explore further.

9 Conclusions

We used NSGA-II, MAP-Elites, MOME, $(\mu + \lambda)$ selection, and simulated annealing to search for SMILES strings representing molecules with desirable NLO qualities that could produce an effective electro-optic modulator. Objectives included maximization of the ratio of first-to-second hyperpolarizability (β/γ), constraining the HOMO-LUMO gap and linear polarizability to target ranges, and minimization of total energy per atom. Results show that with a fine-grained archive, MOME covers the broadest range of structurally diverse molecules (in terms of atom and bond count), and these molecules produce the largest global hypervolume. NSGA-II also produced a decent hypervolume score and performed well on individual objectives, but scores poorly on QD/MOQD metrics. The performance of $(\mu + \lambda)$ also seemed good, as its (β/γ) scores were higher than all others, but this accomplishment came at the expense of the other objectives, meaning that the molecules produced are not useful NLO molecules, despite a high hypervolume score. We will explore the vast array of molecules produced by all methods to assess their utility, and further investigate how to use these algorithms to guide the search for molecules with desired properties.

Acknowledgments

The authors acknowledge that Generative AI (Claude) was used to refine the `matplotlib` code that produced all the result figures.

References

- [1] Hans-Georg Beyer and Hans-Paul Schwefel. 2002. Evolution strategies - A comprehensive introduction. *Nat. Comput.* 1, 1 (2002), 3–52. <http://dblp.uni-trier.de/db/journals/nc/1.html#BeyerS02>
- [2] David M. Bishop. 1998. *Molecular Vibration and Nonlinear Optics*. John Wiley & Sons, Ltd, 1–40. [arXiv:https://onlinelibrary.wiley.com/doi/10.1002/9780470141632.ch1](https://onlinelibrary.wiley.com/doi/10.1002/9780470141632.ch1) doi:10.1002/9780470141632.ch1
- [3] J. Blank and K. Deb. 2020. pymoo: Multi-Objective Optimization in Python. *IEEE Access* 8 (2020), 89497–89509.

[4] Antoine Cully, Jeff Clune, Danesh Tarapore, and Jean-Baptiste Mouret. 2015. Robots that can adapt like animals. *Nature* 521, 7553 (2015), 503–507. doi:10.1038/NATURE14422

[5] Larry Dalton, Bruce Robinson, Alex Jen, Philip Ried, Bruce Eichinger, Sei-Hum Jang, Jingdong Luo, Sen Liu, Yi Liao, Kimberly Firestone, Nishant Bhatambrekar, and Denise Bale. 2004. Organic electro-optic materials. *Proceedings of SPIE - The International Society for Optical Engineering* 5621 (12 2004). doi:10.1117/12.584102

[6] P. Dastmalchi, A. Haddadpour, and G. Veronis. 2014. 11 - Nanophotonics: devices for manipulating light at the nanoscale. In *Nanolithography*, Martin Feldman (Ed.). Woodhead Publishing, 376–398. doi:10.1533/9780857098757.376

[7] K. Deb, A. Pratap, S. Agarwal, and T. Meyarivan. 2002. A fast and elitist multiobjective genetic algorithm: NSGA-II. *IEEE Transactions on Evolutionary Computation* 6, 2 (2002), 182–197. doi:10.1109/4235.996017

[8] Kathryn A. Dowsland. 1993. *Modern Heuristic Techniques for Combinatorial Problems*. John Wiley & Sons, Inc., USA, 20–69.

[9] Matthew C. Fontaine and Stefanos Nikolaidis. 2021. Differentiable quality diversity. In *Proceedings of the 35th International Conference on Neural Information Processing Systems (NIPS '21)*. Curran Associates Inc., Red Hook, NY, USA, Article 768, 13 pages.

[10] Tomoya Hömberg, Sanaz Mostaghim, Satoru Hiwa, and Tomoyuki Hiroyasu. 2024. Optimized Drug Design using Multi-Objective Evolutionary Algorithms with SELFIES. In *2024 IEEE Congress on Evolutionary Computation (CEC)*. 1–8. doi:10.1109/CEC60901.2024.10611870

[11] Tomáš Hrvínak, Miroslav Medved, Wojciech Bartkowiak, and Robert Zalešný. 2022. Hyperpolarizabilities of Push-Pull Chromophores in Solution: Interplay between Electronic and Vibrational Contributions. *Molecules* 27, 24 (2022). doi:10.3390/molecules27248738

[12] David R. Kanis, Mark A. Ratner, and Tobin J. Marks. 1994. Design and construction of molecular assemblies with large second-order optical nonlinearities. Quantum chemical aspects. *Chemical Reviews* 94, 1 (1994), 195–242. arXiv:https://doi.org/10.1021/cr00025a007 doi:10.1021/cr00025a007

[13] Henry A. Kurtz, James J. P. Stewart, and Kenneth M. Dieter. 1990. Calculation of the nonlinear optical properties of molecules. *Journal of Computational Chemistry* 11, 1 (1990), 82–87. arXiv:https://onlinelibrary.wiley.com/doi/pdf/10.1002/jcc.540110110 doi:10.1002/jcc.540110110

[14] M.G. Kuzyk. 2001. Quantum limits of the hyper-Rayleigh scattering susceptibility. *IEEE Journal of Selected Topics in Quantum Electronics* 7, 5 (2001), 774–780. doi:10.1109/2944.97938

[15] Mark G. Kuzyk. 2000. Fundamental limits on third-order molecular susceptibilities. *Opt. Lett.* 25, 16 (Aug 2000), 1183–1185. doi:10.1364/OL.25.001183

[16] Mark G. Kuzyk. 2000. Physical Limits on Electronic Nonlinear Molecular Susceptibilities. *Phys. Rev. Lett.* 85 (Aug 2000), 1218–1221. Issue 6. doi:10.1103/PhysRevLett.85.1218

[17] Greg Landrum. 2010. *RDKit: Open-source cheminformatics*. <https://www.rdkit.org>

[18] S. R. Marder, D. N. Beratan, and L.-T. Cheng. 1991. Approaches for Optimizing the First Electronic Hyperpolarizability of Conjugated Organic Molecules. *Science* 252, 5002 (1991), 103–106. <http://www.jstor.org/stable/2875581>

[19] Seth R Marder, Bernard Kippelen, Alex K-Y Jen, and Nasser Peyghambarian. 1997. Design and synthesis of chromophores and polymers for electro-optic and photorefractive applications. *Nature* 388, 6645 (1997), 845–851. doi:10.1038/42190

[20] Dominic Mashak and Steven Alexander. 2025. Finding Molecules with Large Hyperpolarizabilities. In *MATCH Commun. Math. Comput. Chem.*, Vol. 94. MATCH Commun. Math. Comput. Chem., 633–644. Issue 3. doi:10.46793/match94-3.25824

[21] Dominic Mashak and Steven Alexander. 2025. Finding Molecules with Specific Properties: Simulated Annealing vs. Evolution. In *Proceedings of the Genetic and Evolutionary Computation Conference Companion* (NH Malaga Hotel, Malaga, Spain) (GECCO '25 Companion). Association for Computing Machinery, New York, NY, USA, 759–762. doi:10.1145/3712255.3726635

[22] Dominic Mashak and S. A. Alexander. 2025. Benchmarking Hartree-Fock and DFT for Molecular Hyperpolarizability: Implications for Evolutionary Design. arXiv:2511.17767 [physics.chem-ph] <https://arxiv.org/abs/2511.17767>

[23] Nicholas Metropolis, Arianna W. Rosenbluth, Marshall N. Rosenbluth, Augusta H. Teller, and Edward Teller. 1953. Equation of State Calculations by Fast Computing Machines. *The Journal of Chemical Physics* 21, 6 (06 1953), 1087–1092. doi:10.1063/1.1699114

[24] R.A. Minasian. 2005. Modulation and Demodulation of Optical Signals. In *Encyclopedia of Modern Optics*, Bob D. Guenther and Duncan G. Steel (Eds.). Elsevier, Oxford, 129–138. <https://www.sciencedirect.com/reference/9780123693952/encyclopedia-of-modern-optics>

[25] Jean-Baptiste Mouret and Jeff Clune. 2015. Illuminating search spaces by mapping elites. arXiv:1504.04909 [cs.AI] <https://arxiv.org/abs/1504.04909>

[26] Lucjan Piela. 2020. The Molecule Subject to Electric or Magnetic Fields. In *Ideas of Quantum Chemistry (Third Edition)* (third edition ed.), Lucjan Piela (Ed.). Elsevier, 253–335. doi:10.1016/B978-0-44-464248-6.00012-0

[27] Thomas Pierrot, Guillaume Richard, Karim Beguir, and Antoine Cully. 2022. Multi-objective quality diversity optimization. In *Proceedings of the Genetic and Evolutionary Computation Conference* (Boston, Massachusetts) (GECCO '22). Association for Computing Machinery, New York, NY, USA, 139–147. doi:10.1145/3512290.3528823

[28] Justin K. Pugh, L. B. Soros, Paul A. Szerlip, and Kenneth O. Stanley. 2015. Confronting the Challenge of Quality Diversity. In *Proceedings of the 2015 Annual Conference on Genetic and Evolutionary Computation* (Madrid, Spain) (GECCO '15). Association for Computing Machinery, New York, NY, USA, 967–974. doi:10.1145/2739480.2754664

[29] Javier Pérez-Moreno, Sheng-Ting Hung, Mark G. Kuzyk, Juefei Zhou, Shiva K. Ramini, and Koen Clays. 2011. Experimental verification of a self-consistent theory of the first-, second-, and third-order (non)linear optical response. *Physical Review A* 84, 3 (Sept. 2011). doi:10.1103/physreva.84.033837

[30] M. Blanca Ros. 2008. Organic Materials for Nonlinear Optics. In *Engineering of Crystalline Materials Properties*, Juan J. Novoa, Dario Braga, and Lia Addadi (Eds.). Springer Netherlands, Dordrecht, 375–390.

[31] Bahaa E. A. Saleh and Malvin Carl Teich. 1991. *Electro-Optics*. John Wiley & Sons, Ltd, NY, Chapter 18, 696–736. arXiv:https://onlinelibrary.wiley.com/doi/pdf/10.1002/0471213748.ch18 doi:10.1002/0471213748.ch18

[32] K. D. Singer, J. E. Sohn, L. A. King, H. M. Gordon, H. E. Katz, and C. W. Dirk. 1989. Second-order nonlinear-optical properties of donor- and acceptor-substituted aromatic compounds. *J. Opt. Soc. Am. B* 6, 7 (Jul 1989), 1339–1350. doi:10.1364/JOSAB.6.001339

[33] Philip A. Sullivan and Larry R. Dalton. 2010. Theory-Inspired Development of Organic Electro-optic Materials. *Accounts of Chemical Research* 43, 1 (2010), 10–18. arXiv:https://doi.org/10.1021/ar800264w doi:10.1021/ar800264w PMID:19663413.

[34] Qiming Sun, Xing Zhang, Samragni Banerjee, Peng Bao, Marc Barbry, Nick S. Blunt, Nikolay A. Bogdanov, George H. Booth, Jia Chen, Zhi-Hao Cui, Janus J. Eriksen, Yang Gao, Sheng Guo, Jan Hermann, Matthew R. Hermes, Kevin Koh, Peter Koval, Susi Lehtola, Zhendong Li, Junzi Liu, Narbe Mardirossian, James D. McClain, Mario Motta, Bastien Mussard, Hung Q. Pham, Artem Pulkkin, Wirawan Purwanto, Paul J. Robinson, Enrico Ronca, Elvira R. Sayfutyarova, Maximilian Scheurer, Henry F. Schurkus, James E. T. Smith, Chong Sun, Shi-Ning Sun, Shiv Upadhyay, Lucas K. Wagner, Xiao Wang, Alec White, James Daniel Whitfield, Mark J. Williamson, Sebastian Wouters, Jun Yang, Jason M. Yu, Tianyu Zhu, Timothy C. Berkelbach, Sandeep Sharma, Alexander Yu. Sokolov, and Garnet Kin-Lic Chan. 2020. Recent developments in the PySCF program package. *The Journal of Chemical Physics* 153, 2 (07 2020), 024109. doi:10.1063/5.0006074

[35] Attila Szabó and Neil S. Ostlund. 1996. Modern quantum chemistry : introduction to advanced electronic structure theory. <https://api.semanticscholar.org/CorpusID:94743139>

[36] Peter J. M. van Laarhoven and Emile H. L. Aarts. 1987. Simulated Annealing: Theory and Applications. In *Mathematics and Its Applications*. Springer. <https://link.springer.com/book/10.1007/978-94-015-7744-1>

[37] Jonas Verhelten. 2022. Graph-based molecular Pareto optimisation. *Chem. Sci.* 13 (2022), 7526–7535. Issue 25. doi:10.1039/D2SC00821A

[38] Jonas Verhelten and Jeriek Van den Abeele. 2020. Illuminating elite patches of chemical space. *Chem. Sci.* 11 (2020), 11485–11491. Issue 42. doi:10.1039/D0SC03544K

[39] David Weininger. 1988. SMILES, a chemical language and information system. 1. Introduction to methodology and encoding rules. *Journal of Chemical Information and Computer Sciences* 28, 1 (1988), 31–36. arXiv:https://doi.org/10.1021/ci00057a005 doi:10.1021/ci00057a005

[40] Eckart Zitzler and Lothar Thiele. 1998. Multiobjective Optimization Using Evolutionary Algorithms - A Comparative Case Study. In *Proceedings of the 5th International Conference on Parallel Problem Solving from Nature (PPSN V)*. Springer-Verlag, Berlin, Heidelberg, 292––304.

[41] E. Zitzler, L. Thiele, M. Laumanns, C.M. Fonseca, and V.G. da Fonseca. 2003. Performance assessment of multiobjective optimizers: an analysis and review. *IEEE Transactions on Evolutionary Computation* 7, 2 (2003), 117–132. doi:10.1109/TEVC.2003.810758